



1 **1 km Monthly Precipitation and Temperatures Dataset for China**
2 **from 1952 to 2019 based on a Brand-New and High-Quality**
3 **Baseline Climatology Surface**

4 **Haibo Gong^{1,2,3,4,5}, Xueqiao Xiang^{1,2,3,4,5}, Huiyu Liu*^{1,2,3,4,5}, Xiaojuan Xu^{1,2,3,4,5},**
5 **Fusheng Jiao^{1,2,3,4,5}, Zhenshan Lin^{1,2,3,4,5}**

6 ¹Jiangsu Center for Collaborative Innovation in Geographical Information Resource Development
7 and Application, Nanjing Normal University, Nanjing, 210023, China

8 ²Key Laboratory of Virtual Geographic Environment (Nanjing Normal University), Ministry of
9 Education, Nanjing, 210023, China

10 ³State Key Laboratory Cultivation Base of Geographical Environment Evolution (Jiangsu
11 Province), Nanjing Normal University, Nanjing, 210023, China

12 ⁴College of Geography Science, Nanjing Normal University, Nanjing 210023, China

13 ⁵Jiangsu Key Laboratory of Environmental Change and Ecological Construction, Nanjing Normal
14 University, Nanjing 210023, China

15

16

17

18

19

20

21 **Correspondence:** Dr Huiyu Liu, Nanjing Normal University, No 1 Wenyuan Road, Qixia

22 District, Nanjing, China. Tel: (+86) 18951838599; E-mail: liuhuiyu@njnu.edu.cn



23 Abstract

24 Long-term climate data and high-quality baseline climatology surface with high resolution are
25 highly essential to multiple fields in climatological, ecological, hydrological, and environmental
26 sciences. Here, we created a brand-new baseline climatology surface (ChinaClim_baseline) and
27 developed a 1km monthly precipitation and temperatures dataset in China during 1952-2019
28 (ChinaClim_timeseries). Thin plate spline (TPS) algorithm in each month with different model
29 formulations by accounting for satellite-driven products, was used to generate ChinaClim_baseline
30 and monthly climate anomaly surface. Meanwhile, climatologically aided interpolation (CAI) was
31 used to superimpose monthly anomaly surface with ChinaClim_baseline to generate
32 ChinaClim_timeseries. Our results showed that ChinaClim_baseline exhibited very high
33 performance. For precipitation estimation, the values of all R^2 were over 0.860, and the values of
34 $RMSEs$ and $MAEs$ were 8.149 mm~21.959 mm and 2.787~14.125 mm, respectively. Annual average,
35 maximum and minimum temperature had average R^2 of 0.967~0.992, $MAEs$ of 0.321~0.785 °C, and
36 $RMSEs$ between 0.485 °C and 1.233 °C for all months. ChinaClim_baseline performed much better
37 than WorldClim2 and CHELSA, especially in summer months and the regions with low-density
38 weather stations in temperate continental and high cold Tibetan Plateau climate zones. For
39 ChinaClim_timeseries, precipitation had an average R^2 of 0.699~0.923, an average $RMSE$ between
40 7.449 mm and 56.756 mm, and an average of MAE of 4.263~40.271 mm for all months. Temperature
41 elements had an average R^2 of 0.936~0.985, an average $RMSE$ between 0.807 °C and 1.766 °C, and
42 an average MAE of 0.548~1.236 °C for all months. Compared with Peng's climate surface and
43 CHELSAcruts, R^2 increased by approximately 6 %, $RMSE$ and MAE decreased by approximately
44 15 % for precipitation; R^2 of temperatures had no obvious changes, but $RMSE$ and MAE decreased
45 by 8.37~34.02 %. The results showed that the performance of ChinaClim_timeseries in interannual
46 variations performed much better than other datasets, thanks to the help of ChinaClim_baseline and
47 satellite-driven products. Remarkably, ChinaClim_baseline did not greatly improve precipitation
48 estimation, but it deeply improved temperature estimation; the satellite-driven TRMM3B43
49 anomaly can greatly improve precipitation estimation, while the LST anomaly did not substantially
50 improve temperature estimation. ChinaClim_baseline can be used as an excellent baseline



51 climatology surface for obtaining high-quality and long-term climate datasets from past to future.
52 In the meantime, ChinaClim_timeseries of 1km spatial resolution based on ChinaClim_baseline, is
53 very suitable for investigating the spatial-temporal climate changes and their impacts on eco-
54 environmental systems in China. Now, ChinaClim_baseline is available at
55 <https://doi.org/10.5281/zenodo.4287824> (Gong, 2020a), ChinaClim_timeseries of precipitation is
56 available at <https://doi.org/10.5281/zenodo.4288388> (Gong, 2020b), ChinaClim_timeseries of
57 maximum temperature is available at <https://doi.org/10.5281/zenodo.4288390> (Gong, 2020c) and
58 ChinaClim_timeseries of minimum temperature is available at
59 <https://doi.org/10.5281/zenodo.4288392> (Gong, 2020d).

60
61
62
63
64
65
66
67
68
69
70
71
72
73
74
75
76
77
78



79 **1 Introduction**

80 Long-term information on climatic conditions is pivotal for understanding global changes including
81 atmospheric movements, vegetation dynamics, soil moisture, and other related scientific and
82 application fields which are conducted at a resolution of ~1 km (Chaney et al., 2014; Gao et al.,
83 2018; Hijmans et al., 2005; Karger et al., 2017; Liu et al., 2016; New et al., 2002; Pfister et al., 2020;
84 Wagner and Wolfgang, 2003). However, global climate datasets often only represent climatic
85 variation at spatial resolutions of 0.25~1 degree, such as Climatic Research Unit: CRU (Harris et
86 al., 2014), The European Centre for Medium-Range Weather Forecast (ECWMF) Climatic
87 reanalysis: ERA (Sterl et al., 1998), Global Precipitation and temperature: UDEL (Lawrimore et al.,
88 2011), The Berkeley Earth Surface Temperatures: BEST (Muller et al., 2013), Global Precipitation
89 Climatology Centre: CPCC (Becker et al., 2013). Thus, high resolution gridded climate data is
90 urgently needed for studying global and regional climate change and its influences (Hamann et al.,
91 2015; Hijmans et al., 2005; Karger et al., 2017).

92 A variety body of work was motivated to obtain high resolution gridded climate data with spatial
93 interpolation methods and statistical downscaling (Li and Shao, 2010; Wu and Li, 2013; Hartkamp
94 et al., 1999; Boer et al., 2001). Spatial interpolation methods including Kriging, Inverse Distance
95 Weighting and Spline were widely applied in the estimates of climate elements (temperature,
96 precipitation, vapor pressure, solar radiation and wind speed) at arbitrary spatial resolution. Among
97 them, thin plate spline (TPS) interpolation was considered to perform well in generating grids of
98 climate elements (Boer et al., 2001; Hartkamp et al., 1999; Hijmans et al., 2005; Hutchinson, 1995;
99 Fick et al., 2017). However, for the estimates of long-term monthly climate surface, recent studies
100 have shown that climatologically aided interpolation (CAI) employing the temporal anomaly
101 surface and an accurate baseline climatology surface with high resolution, is well suited for
102 producing long-term climate datasets than direct interpolation using original weather stations
103 (Abatzoglou et al., 2018; Becker et al., 2013; C. Vega et al., 2017; Karger et al., 2017; Mosier et al.,
104 2014; Peng et al., 2019; Willmott and Robeson, 2010). Remarkably, the quality of monthly climate
105 surface, generated by CAI method, was thought to be determined by the baseline climatology
106 surface (Gao et al., 2018; Peng et al., 2019). Baseline climatology surface, also called 30-Year



107 Normals, described the average monthly conditions over the most recent three full decades. Previous
108 efforts have developed many high-quality baseline climatology surfaces with a resolution of ~1km,
109 such as WorldClim (Hijmans et al., 2005), WorldClim2 (Fick et al., 2017) and CHELSA (Karger et
110 al., 2017) for global land surface, PRISM (Daly et al., 2002; Daly et al., 2008) and Daymet
111 (Thornton et al., 1997) for North America. Although these baseline climatology surfaces are widely
112 used for basic and applied studies such as climatological, ecological, hydrological, and
113 environmental fields (Belda et al., 2017; Ray et al., 2015), a gap between these gridded climate
114 datasets and weather stations was still observed in many areas with complex topography and sharp
115 gradient changes due to lacking of sufficient weather stations information (New et al., 2002; Fick et
116 al., 2017). Data quality of WorldClim was thought to depend on local climate variability, quality
117 and density of observations, and the degree of the fitted spline (Hijmans et al., 2005). Unfortunately,
118 for currently available high-quality baseline climatology surface with high-resolution covering
119 China like WorldClim2 and CHELSA, only a small part of weather stations (323 and 228 stations
120 for WorldClim2 and CHELSA respectively) were employed to generate baseline climatology
121 surface. Weather stations are the most reliable source of the estimation of temperatures and
122 precipitation, and thus more weather stations can provide more accurate point measure information.
123 In fact, we can use a dataset of 30-year average climate (1980-2010) containing more than 2000
124 weather stations from China Meteorological Data Service Center (CMD: <http://cdc.nmic.cn>) and
125 Central Weather Bureau (www.cwb.gov.tw), which are bound to greatly improve the quality of the
126 baseline climatology surface for China.

127 Previous efforts have shown that the estimate of climate elements is likely to be improved by using
128 satellite-driven products in the regions with insufficient weather station density (or quality)
129 (Deblauwe et al., 2016; Jin and Dickinson, 2010; Mildrexler et al., 2011). With the development of
130 remote sensing and geographic information technology, satellite-driven climate grid products
131 become the optimum source in measuring climate elements at regional and global scales (Huffman
132 et al., 2010; Michaelides et al., 2009; Siuki et al., 2017). The TRMM Multisatellite Precipitation
133 Analysis (TMPA) monthly 3B43 products have been utilized extensively to provide valuable
134 precipitation information in areas with sparse weather stations over the last two decades (Biasutti et
135 al., 2012; Huffman et al., 2010; Simpson et al., 1996). Land surface temperature (LST) is now



136 available from satellite-borne instruments, which is widely incorporated in estimating air
137 temperature (Kilibarda et al., 2014, Yao et al., 2020). Both WorldClim2 and CHELSA have not
138 considered satellite-driven precipitation products and CHELSA have not considered satellite-driven
139 temperature products. Despite many studies have shown these TRMM3B43 and LST products can
140 increase the accuracy of the estimates of precipitation and temperature (Kilibarda et al., 2014;
141 Kolios and Kalimeris, 2020; Yao et al., 2020), they are only available after 1997 and 2000
142 respectively, which is not long enough for the long-term ecological and hydrological analyses and
143 modeling. Therefore, there is an urgent need to combine satellite-driven TRMM3B43 and LST in
144 climate interpolation to generate a brand-new and higher-quality baseline climatology surface
145 (ChinaClim_baseline), and further to combine ChinaClim_baseline to create a high-quality monthly
146 time series of precipitation and temperatures dataset with high spatial resolution for China
147 (ChinaClim_timeseries) from 1952 to 2019 with CAI method.
148 Specifically, the objectives of this work are: (1) to create a brand-new and higher-quality baseline
149 climatology surface for China (ChinaClim_baseline). (2) to generate a 1 km monthly temperatures
150 and precipitation dataset in China for the period of 1952-2019 (ChinaClim_timeseries).

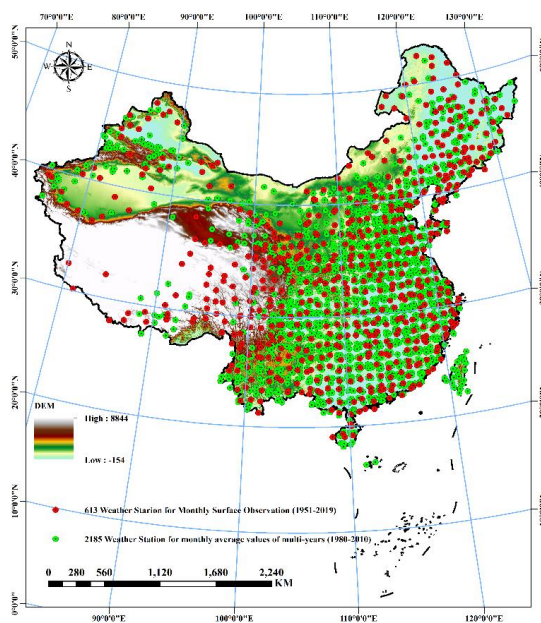
151
152
153
154
155
156
157
158
159
160



161 2 Data

162 2.1 Weather observation stations

163 Dataset of 30-year average climate (1980-2010) was obtained from two sources, 2438 weather
164 stations from CMD and 25 weather stations from Central Weather Bureau. Dataset of monthly
165 surface observation values drawn from 613 weather stations for the period of 1952-2019 was
166 collected from CMD. Influenced by the monsoon and Tibetan Plateau, four climate zones (Fig.1:
167 Temperate continental, Temperate monsoonal, High cold Tibetan Plateau, and Subtropical-tropical
168 monsoonal climate zones) have experienced various climate changes in both precipitation and
169 temperature (He et al 2018), and so, weather stations were divided into four zones to assess the
170 accuracy of data products in the areas with sparse and dense weather stations.



171
172 Figure1. The spatial distribution of weather stations in four climate zones (i.e. Temperate continental, Temperate monsoonal,
173 High cold Tibetan Plateau, and Subtropical-tropical monsoonal climate zones) of China. (Map created by myself)

174 2.2 Version 7 TRMM3B43 datasets and Land Surface Temperature

175 The Tropical Rainfall Measuring Mission (TRMM), a joint project by the National Aeronautics and



176 Space Administration (NASA) of the United States and the Japan Aerospace Exploration Agency
177 (JAXA), was launched in November 1997 to monitor and investigate the tropical and subtropical
178 rain system (Huffman et al., 2010; Simpson et al., 1996). The Version 7 monthly TRMM3B43 in
179 NetCDF format was downloaded from <https://mirador.gsfc.nasa.gov>, with a spatial resolution of
180 0.25 degree over a latitude range from 50°S to 50°N during 1998-2019. It was resampled to ~1km
181 spatial resolution via bilinear interpolation, and was averaged to get monthly and yearly
182 TRMM3B43. Land surface temperature (LST) was compiled from Moderate Resolution Imaging
183 Spectroradiometer (MODIS). Mean night and day LST values were extracted from ~1 km resolution
184 MOD11A2 images, averaged by month and year from 2001 to 2019. The MOD11A2 images can be
185 freely available at <https://ladsweb.modaps.eosdis.nasa.gov>.

186 2.3 Elevation and distance to the nearest coast

187 Elevation data with a spatial resolution of 30 m from Shuttle Radar Topography Mission (STRM)
188 (data available at <http://srtm.csi.cgiar.org/>) was aggregated to ~1km spatial resolution. Coastline
189 dataset was downloaded from <https://www.ngdc.noaa.gov/mgg/shorelines/>. We calculated the
190 distance to the nearest coast using Euclidean distance in ArcGIS 10.2 with the fine coastline datasets.

191 2.4 Baseline climatology surfaces and monthly climate datasets used for 192 comparison

193 Two baseline climatology surfaces as WorldClim2 (Fick et al., 2017) and CHELSA (Karger et al.,
194 2017) with 1km spatial resolution were used to compare the accuracy of ChinaClim_baseline.
195 WorldClim2 was interpolated with ANUSPLIN (Hutchinson, 1995), a method that fits thin plate
196 splines through station data in three dimensions: latitude, longitude, and elevation. WorldClim2 can
197 be accessed online at www.worldclim.org. CHELSA is essentially a quasi-mechanistical statistical
198 downscaling of the ERA-Interim reanalysis, with the temperature downscaling based on mean lapse
199 rates and elevation, and the precipitation algorithm using geographic predictors including wind
200 fields, exposure, and boundary layer height (Karger et al., 2017). CHELSA can be freely available
201 at www.chelsa-climate.org.



202 We also collected two long-term climate datasets with high resolution. One is the recently published
203 Peng's climate surfaces (Peng et al., 2019). This climate dataset was spatially downscaled from 30'
204 Climatic Research Unit (CRU) time series dataset with the baseline climatology surface of
205 WorldClim2 using CAI. This is a 1km dataset of monthly air temperatures at 2m and precipitation
206 for China in the period of 1901-2017. Peng's climate surface can be freely available at
207 www.zenodo.org. The other is CHELSAcruts, a delta changes monthly climate dataset for the years
208 1901-2016 including mean monthly maximum temperatures, mean monthly minimum temperatures,
209 and monthly precipitation sum. Anomalies of the CRU TS 4.01 dataset were interpolated between
210 all CRU TS grid cells and are then added (for temperature variables) or multiplied (in case of
211 precipitation) to high resolution climate data from CHELSA (Karger et al., 2017). CHELSAcruts
212 can be freely available at www.chelsa-climate.org.

213
214
215
216
217
218
219
220
221
222
223
224
225



226 3 Method

227 3.1 Creation of baseline climatology surface over China 228 (ChinaClim_baseline)

229 The monthly averaged precipitation and temperatures of multi-years (1980-2010) were interpolated
230 with the thin plate spline (TPS) from R packages “fields”. Spline models for the N observed data
231 values z_i are fit as the following:

$$232 \quad z_i = f(x_i) + a^T y_i + \lambda \quad (i = 1, \dots, N) \quad (1)$$

233 Where f is a smooth function of the spline independent variable x_i , a is a vector of linear
234 coefficients for the independent covariates y_i . In this study, we considered longitude, latitude,
235 elevation, distance to the nearest coast and satellite-driven variables to construct TPS model. We
236 listed climate elements and variables used in TPS model for estimating ChinaClim_baseline in Table
237 1. It is worth noting that longitude, latitude and elevation were set as spline independent variables
238 and the other variables were used as either independent spline variables or linear covariates.
239 Especially, Elevation (m) was divided by 1000 following scaling recommendations by Hutchinson
240 (1995). Precipitation values were square root transformed prior to fitting following
241 recommendations by Hutchinson and Xu (2013). Moreover, TRMM3B43 contained a latitude range
242 from 50°S to 50°N, so we constructed TPS model including TRMM3B43 in the area south of 50°N
243 and constructed TPS models without TRMM3B43 in the area north of 49°N. The 1° overlap area
244 ensures that baseline climatology surface of the two areas can be better merged by weighting
245 estimates inversely proportional to distance from each region’s border (Hijmans et al., 2005; New
246 et al., 2002).

247 Specifically, the process for generating ChinaClim_baseline can be described as follows (Fig.2):

248 (1) After removing duplicate and invalid weather stations, the remaining were split into 10 folds in
249 each climate zones to assure that there was enough train and test data for each climate zones to build
250 and verify the model, and thus to avoid spatial autocorrelation.

251 (2) We randomly extracted 9 folds weather stations in each climate zones and combined them into
252 a new train data set. The remained were combined as test data set to valid the accuracy of model.



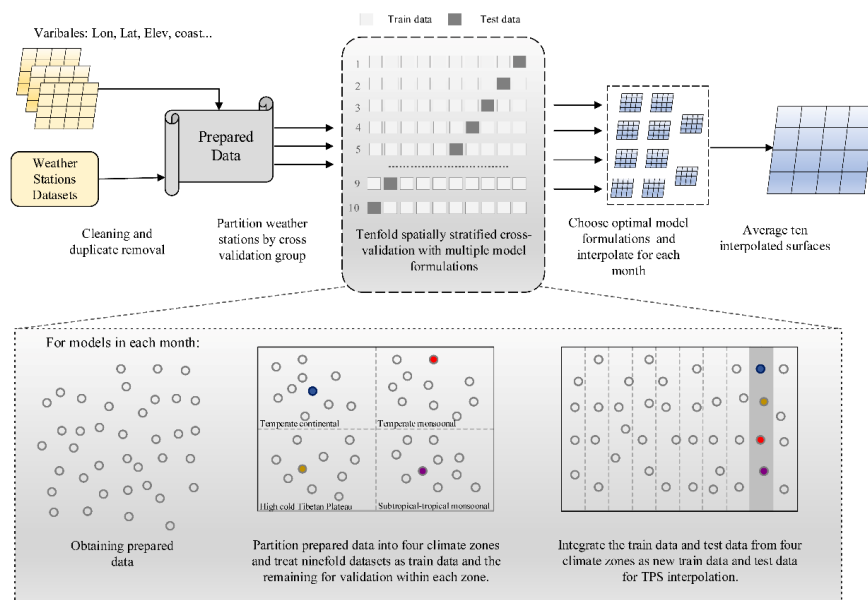
253 (3) 14 model formulations for each month were tried using different combinations of variables to
 254 generate baseline climatology surface (Model formulations about Longitude, Latitude, Elevation,
 255 Distance to the nearest coast and Satellite-driven TRMM3B43 and LST described in Table S1).
 256 (4) Each surface for each month was created by selecting only the model with the highest average
 257 R^2 value.
 258 (5) Repeat steps 2 to 4 for 10 times, and final baseline climatology surface (ChinaClim_baseline)
 259 was created by averaging ten surfaces.

260 Table 1. Climate elements and variables used in TPS model for creating baseline climatology and anomaly surface.

Climate elements	Unit	Variables used in TPS models
Precipitation	mm	Lon, Lat, Elev, Coast, Trmm_m, Trmm_y
Minimum temperature	°C	Lon, Lat, Elev, Coast, Lst_nm, Lst_ny
Maximum temperature	°C	Lon, Lat, Elev, Coast, Lst_dm, Lst_dy
Average temperature	°C	Lon, Lat, Elev, Coast, Lst_am, Lst_ay
Precipitation anomaly	mm	Lon, Lat, Elev, Coast, Trmm_a(1998-2019), Base_prep
Minimum temperature anomaly	°C	Lon, Lat, Elev, Coast, Lst_na(2001-2019), Base_tmin
Maximum temperature anomaly	°C	Lon, Lat, Elev, Coast, Lst_da(2001-2019), Base_tmax
Average temperature anomaly	°C	Lon, Lat, Elev, Coast, Lst_aa(2001-2019), Base_tavg

261 Notes: Variables include longitude (Lon), latitude (Lat), elevation (Elev), distance to the nearest coast (Coast), averaged monthly (Trmm_m) and yearly (Trmm_y)
 262 TRMM3B43 during 1998-2019, monthly TRMM anomaly (Trmm_a), MOD11A2 land surface temperature (the day LST, the night LST, and the average of the
 263 day and night LST) during 2001-2019 averaged by month (Lst_dm, Lst_nm, Lst_am) and year (Lst_dy, Lst_ny, Lst_ay), MOD11A2 land surface temperature
 264 anomaly during 2001-2019 (Lst_da, Lst_na, Lst_aa), Baseline precipitation surface (Base_prep), Baseline temperatures surface (Base_tmin, Base_tavg,
 265 Base_tmax). Lon, Lat and Elev were set as spline independent variables and the other variables were set as either independent spline variables or linear covariates

266



267
268
269

Figure2. Workflow for creating baseline climatology surface (ChinaClim_baseline) and monthly anomaly surface of China (adapted from Fick et al., 2017)

270 3.2 Generation of monthly precipitation and temperatures surface for China 271 (ChinaClim_timeseries)

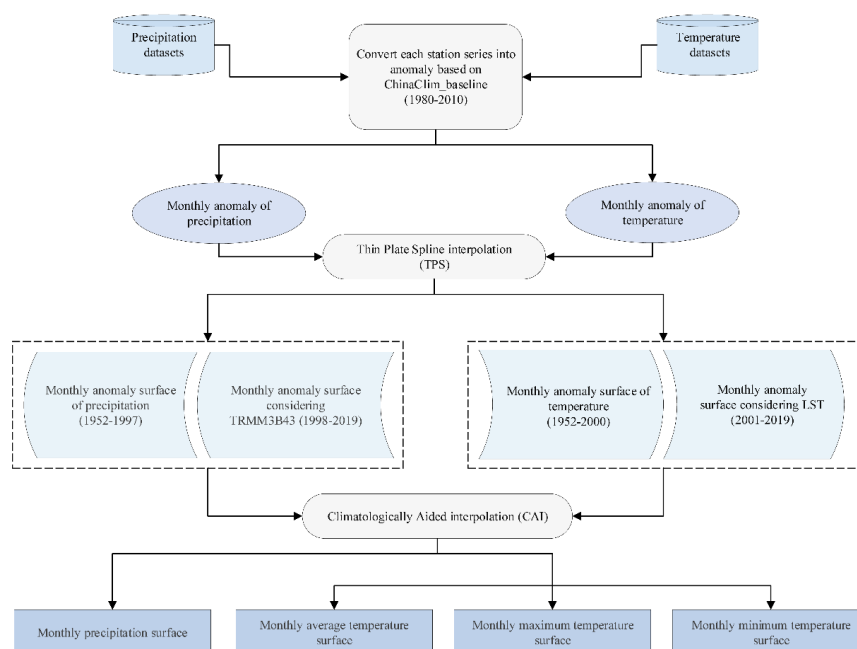
272 CAI method was used to superimpose monthly anomaly surface and baseline climatology surface
273 (ChinaClim_baseline) to produce monthly precipitation and temperatures surface during 1952.01-
274 2019.12 in China (ChinaClim_timeseries) as the following (Fig.3) :

275 Firstly, the anomaly time series was calculated by the difference between the original time series
276 from weather stations and ChinaClim_baseline described in Chapter 3.1.

277 Secondly, similar to the way to obtain ChinaClim_baseline (Fig.2), we applied TPS model to
278 generate monthly anomaly surface from 1952.01 to 2019.12 with a segmented strategy. For monthly
279 anomaly surface (Precipitation: 1952-1997; Temperature: 1952-2000), 7 model formulations were
280 built by using different combinations of variables (Longitude, Latitude, Elevation, Distance to the
281 nearest coast and ChinClim_baseline described in Table S7: Model1-7). Similarly, for monthly
282 anomaly surface during 1998-2019 and 2001-2019 for Precipitation and Temperature, respectively,
283 14 model formulations were constructed using different combinations of variables (Longitude,



284 Latitude, Elevation, Distance to the nearest coast, ChinaClim_baseline and Satellite-driven TRMM
 285 and LST anomaly described in Table S7: Model1-14). Monthly anomaly surface during 1952-2019
 286 was created by selecting only the model with the highest average R^2 value.
 287 Finally, ChinaClim_timeseries was generated by superimposing monthly anomaly surface and
 288 ChinaClim_baseline from 1952.01 to 2019.12.



289
 290 Figure3. Workflow for ChinaClim_timeseries generation based on climatologically aided interpolation (CAI).

291 3.3 Evaluation metrics

292 Three statistic indices including the root mean square error ($RMSE$), mean absolute error (MAE) and
 293 coefficients of determination (R^2) are examined to evaluate the performance of ChinaClim_baseline
 294 and ChinaClim_timeseries.

295
$$RMSE = \sqrt{\frac{\sum_{i=1}^n (P_i - M_i)^2}{n}} \quad (2)$$

296
$$MAE = \frac{\sum_{i=1}^n |P_i - M_i|}{n} \quad (3)$$



297
$$R^2 = \left(\frac{\sum_{i=1}^n (M_i - \bar{M})(P_i - \bar{P})}{\sqrt{\sum_{i=1}^n (M_i - \bar{M})^2 (P_i - \bar{P})^2}} \right)^2 \quad (4)$$

298 Where P_i is the estimates like ChinaClim_baseline/ChinaClim_timeseries in the i th weather station;
299 M_i is the measured value from the i th weather station; n is the number of weather stations; \bar{P} is the
300 average of the estimates like ChinaClim_baseline/ChinaClim_timeseries from n weather stations;
301 \bar{M} is the average of the measured value from n weather stations.

302

303

304

305

306

307

308

309

310

311

312

313

314

315

316

317

318

319



320 4 Results

321 4.1 A brand-new and high-quality baseline climatology surface for China 322 (ChinaClim_baseline)

323 4.1.1 The optimal models and its overall accuracy for ChinaClim_baseline

324 For the estimates of precipitation (Table S2), the models with the highest R^2 in each month all
325 employed satellite-driven TRMM3B43, especially that monthly averaged TRMM (TRMM_m)
326 improve the accuracy in all months, which indicated that TRMM3B43 improved the estimates of
327 precipitation. For all temperature elements included average, maximum and minimum temperature
328 (Table S3-5), models considering LST were superior in most months especially in summer months.
329 Thus, LST could improve the interpolation of temperatures, while LST's ability to improve
330 temperature estimation might be restricted in winter months, especially for average and minimum
331 temperature. Overall, satellite-driven data can improve the estimates of precipitation and
332 temperatures.

333 As shown from Table 3, ChinaClim_baseline exhibited very high performance over independent
334 weather stations. Specifically, for precipitation estimation, the lowest value of R^2 was 0.860 in
335 December, and the highest value was close to 0.98 in March and April, and the values of $RMSEs$
336 and $MAEs$ were 8.149~21.959 mm and 2.787~14.125 mm, respectively. Temperature elements had
337 an average R^2 of 0.967~0.992, an average $RMSEs$ between 0.485 and 1.233 °C, and an average
338 $MAEs$ of 0.321~0.785 °C for all months. Specifically, R^2 of all temperature elements were very high,
339 but the MAE and $RMSE$ of the average temperature were the smallest, followed by the maximum
340 and minimum temperature. Moreover, the temperature estimation performed much better in summer
341 months than in winter months with lower $RMSE$ and MAE .

342
343
344
345
346



347 Table 3. Tenfold cross-validation statistics for ChinaClim_baseline. Coefficients of determination (R^2), root mean
 348 square error ($RMSE$) and mean absolute error (MAE) between observed and baseline climatology surface over
 349 independent weather stations.

		Jan	Feb	Mar	Apr	May	Jun	Jul	Aug	Sep	Oct	Nov	Dec
Precipitation	R^2	0.920	0.950	0.975	0.978	0.966	0.953	0.905	0.899	0.928	0.914	0.899	0.860
	$RMSE$	8.149	8.205	8.547	9.542	14.229	20.378	21.959	21.858	15.543	14.293	11.503	8.801
	MAE	2.787	3.171	4.252	5.392	7.685	11.561	14.125	13.289	8.578	5.732	3.701	2.484
Average temperature	R^2	0.990	0.989	0.989	0.987	0.984	0.982	0.985	0.986	0.988	0.990	0.993	0.991
	$RMSE$	0.902	0.822	0.676	0.576	0.539	0.520	0.498	0.485	0.519	0.580	0.654	0.809
	MAE	0.558	0.523	0.438	0.378	0.360	0.331	0.321	0.322	0.360	0.400	0.454	0.528
Maximum temperature	R^2	0.990	0.986	0.982	0.974	0.968	0.967	0.974	0.979	0.981	0.986	0.992	0.992
	$RMSE$	0.815	0.840	0.787	0.715	0.657	0.649	0.598	0.540	0.550	0.600	0.620	0.738
	MAE	0.464	0.482	0.458	0.425	0.382	0.392	0.366	0.334	0.335	0.343	0.379	0.440
Minimum temperature	R^2	0.985	0.985	0.986	0.984	0.982	0.980	0.983	0.984	0.983	0.986	0.987	0.985
	$RMSE$	1.233	1.106	0.884	0.771	0.719	0.659	0.609	0.618	0.716	0.797	0.934	1.149
	MAE	0.785	0.717	0.603	0.547	0.516	0.447	0.409	0.414	0.496	0.565	0.651	0.773

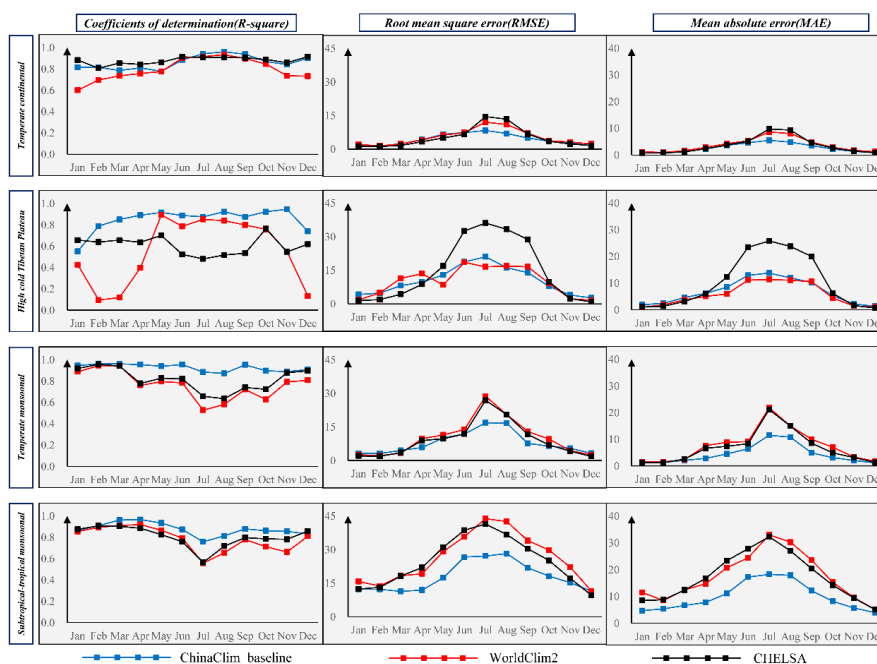
350

351 4.1.2 Comparison of ChinaClim_baseline to WorldClim2 and CHELSA in four climate
 352 zones.

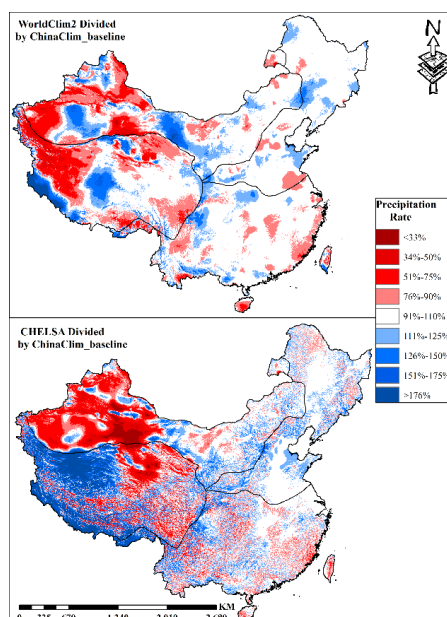
353 To better assess the performance of ChinaClim_baseline, it was compared to two widely recognized
 354 baseline climatology surface with same spatial resolution: WorldClim2 (Fick et al., 2017) and
 355 CHELSA (Karger et al., 2017). The independent weather stations from a tenfold cross-validation
 356 approach were used to diagnose the performance of ChinaClim_baseline, while the independent
 357 weather stations extracted from CMD were used to calculate the accuracy of WorldClim2 and
 358 CHELSA. Considering that both worldClim2 and CHELSA used elevation to estimate temperature
 359 and precipitation, large deviations between the recorded and actual elevation (1 km DEM) in some
 360 weather stations might cause large discrepancy in the estimated and actual precipitation (Fick et al.,
 361 2017). Thus, only these independent weather stations with small deviations (< 200 m) between the
 362 recorded and actual elevation (1 km DEM) were used to assess the accuracy of WorldClim2 and
 363 CHELSA. (Figs 4, 6, 8 and 10). Moreover, spatial differences between ChinaClim_baseline and
 364 WorldClim2 as well as CHELSA for annual total precipitation, annual average temperature, January
 365 minimum temperature, and July maximum temperature were shown in Figs 5, 7, 9, and 11,
 366 respectively.



367 As shown in Fig.4, despite relatively small differences in precipitation accuracy of three baseline
 368 climatology surfaces in Oct-Jun, ChinaClim_baseline greatly improved the accuracy of
 369 precipitation in Jul-Sep with lower *RMSE* and *MAE* along with higher R^2 in the all four climate
 370 zones. Specifically, in the temperate monsoonal and subtropical-tropical monsoonal zones with
 371 high-density weather stations, compared with precipitation accuracy of WorldClim2 and CHELSA,
 372 the accuracy of ChinaClim_baseline was much higher in most months. In high cold Tibetan Plateau,
 373 the accuracy of CHELSA was the worst with the highest *RMSE* and *MAE* in summer months.
 374 Although the *RMSE* and *MAE* of WorldClim2 were slightly lower than ChinaClim_baseline, its R^2
 375 was by far lower than ChinaClim_baseline with huge seasonal variations. There are some spatial
 376 differences between ChinaClim_baseline and WorldClim2 and CHELSA for annual total
 377 precipitation (Fig.5). WorldClim2 tended to be drier than ChinaClim_baseline in many locations,
 378 especially at higher elevations. CHELSA was pretty wetter in high cold Tibetan Plateau and much
 379 drier in temperate continental than ChinaClim_baseline.



380
 381 Figure 4. The accuracy of ChinaClim_baseline and WorldClim2 and CHELSA for precipitation in the temperate continental, high
 382 cold Tibetan Plateau, temperate monsoonal, and subtropical-tropical monsoonal climate zones.

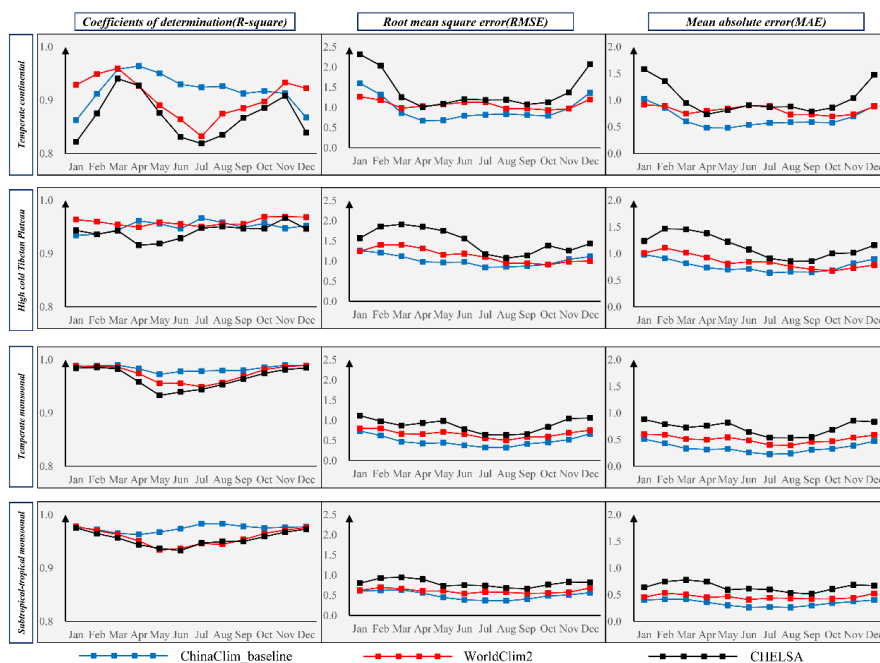


383
384 Figure 5. WorldClim2/ ChinaClim_baseline and CHELSA/ ChinaClim_baseline ratio maps (expressed as percentage) of annual
385 precipitation for China.

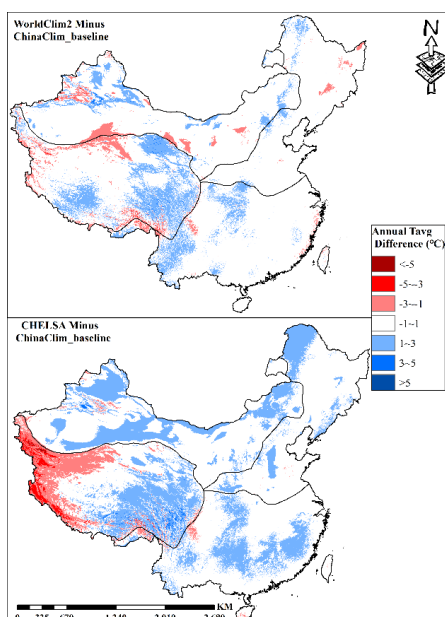
386 For temperature elements included average, maximum and minimum temperature, the performance
387 of ChinaClim_baseline was the most excellent, followed by WorldClim2 and CHELSA (Figs 6, 8,
388 and 10). Although there is no obvious discrepancy in the accuracy of temperature estimation in Oct-
389 Mar among ChinaClim_baseline, WorldClim2, and CHELSA, ChinaClim_baseline improved R^2
390 and greatly reduced $RMSE$ and MAE in Apr-Sep which were during the growing season of most
391 plants. The temperature estimation of ChinaClim_baseline, WorldClim2 and CHELSA in temperate
392 continental and high cold Tibetan Plateau climate zones performed worse (higher $RMSE$ and MAE
393 and lower R^2) relative to subtropical-tropical monsoonal and temperate monsoonal climate zones.
394 However, due to more weather stations and powerful algorithms, ChinaClim_baseline tangibly
395 improved the temperature estimation of WorldClim2 and CHELSA in the above two regions.
396 Moreover, the spatial discrepancy between ChinaClim_baseline and WorldClim2 and CHELSA for
397 temperatures were smaller than precipitation as temperature generally follows relatively simple
398 gradients of latitude and elevation (Fig.5). For annual average temperature, most areas showed small
399 differences within $-1\sim 1$ °C, and worldClim2 and CHELSA were slightly hotter than
400 ChinaClim_baseline. However, for July maximum temperature (Fig.7), they were colder than



401 ChinaClim_baseline except for temperate continental climate zone. In particular, CHELSA was
 402 colder than ChinaClim_baseline in vast high-altitude areas. For January minimum temperature
 403 (Fig.9), WorldClim2 was generally cooler than ChinaClim_baseline and CHELSA was seriously
 404 warmer than ChinaClim_baseline in most high-altitude areas. Overall, there were some spatial
 405 discrepancies between ChinaClim_baseline and WorldClim2 and CHELSA in many areas of China,
 406 especially in low-density weather station regions such as high cold Tibetan Plateau and temperate
 407 continental.

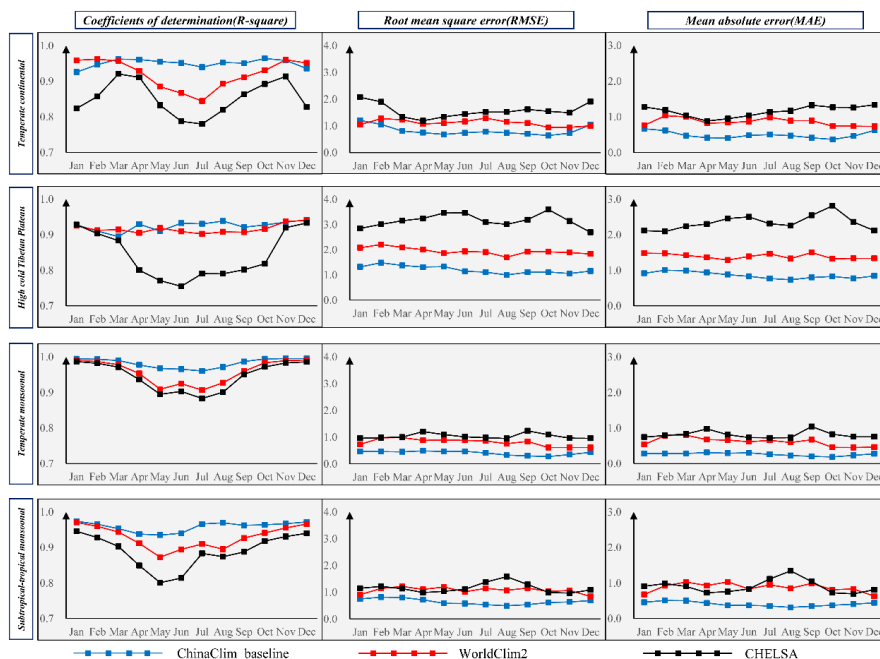


408
 409 Figure 6. The accuracy of ChinaClim_baseline and WorldClim2 and CHELSA for average temperature in the temperate
 410 continental, high cold Tibetan Plateau, temperate monsoonal, and subtropical-tropical monsoonal climate zones.



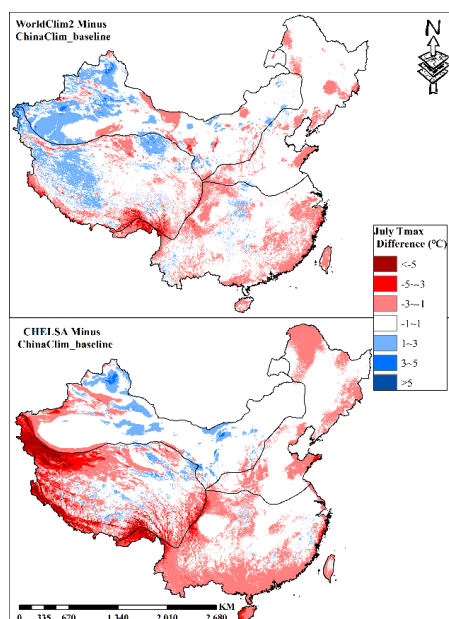
411

412 Figure 7. WorldClim2 - ChinaClim_baseline and CHELSA - ChinaClim_baseline difference maps of annual average temperature
 413 for China.

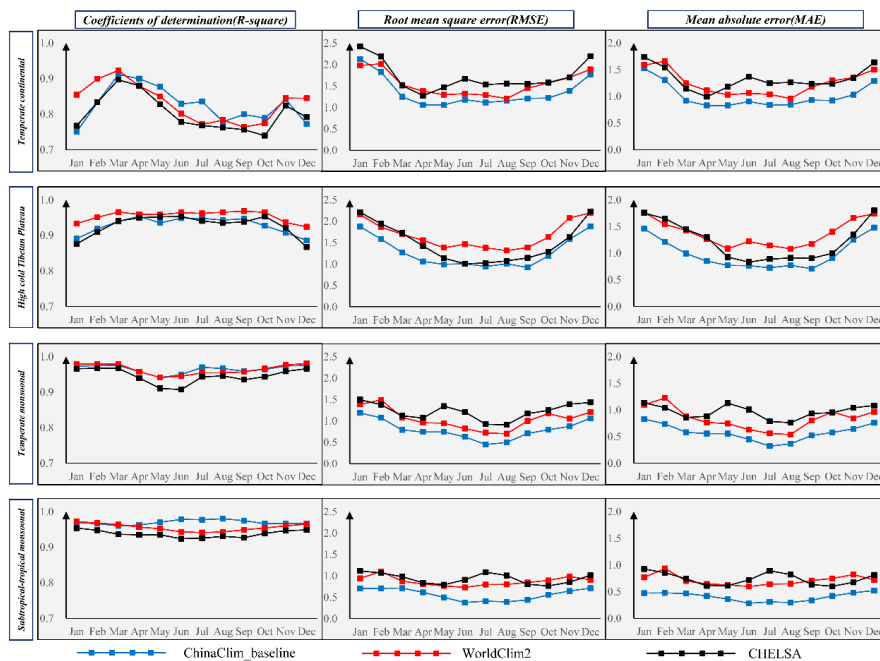


414

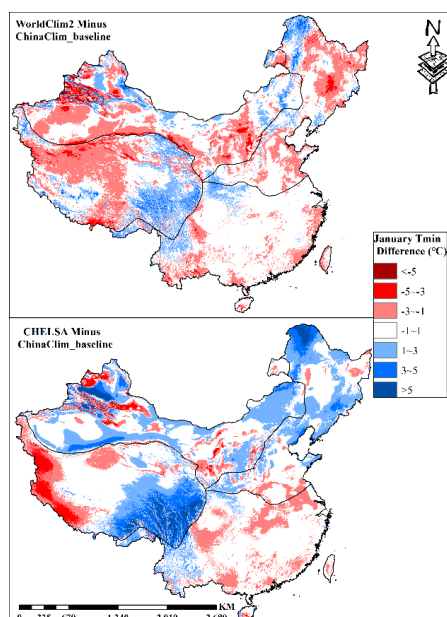
415 Figure 8. The accuracy of ChinaClim_baseline and WorldClim2 and CHELSA for maximum temperature in the temperate
 416 continental, high cold Tibetan Plateau, temperate monsoonal, and subtropical-tropical monsoonal climate zones.



417
 418 Figure 9. WorldClim2 - ChinaClim_baseline and CHELSA - ChinaClim_baseline difference maps of July maximum temperature
 419 for China.



420
 421 Figure 10. The accuracy of ChinaClim_baseline and WorldClim2 and CHELSA for minimum temperature in the temperate
 422 subtropical-tropical monsoonal climate zones.



423

424

425

Figure 11. WorldClim2 - ChinaClim_baseline and CHELSA - ChinaClim_baseline difference maps of January minimum temperature for China.

426

4.2 1km monthly precipitation and temperatures surfaces during 1952-2019

427

(ChinaClim_timeseries)

428

4.2.1 The optimal models and accuracy of ChinaClim_timeseries with seasonal

429

variation

430

Models (Model4, Model5, and Model7) considering baseline climatology surface, showed better

431

performance in all months for precipitation anomaly and temperatures anomaly during 1952-1997

432

and 1952-2000, respectively (Table S12). For precipitation anomaly during 1998-2019, models

433

(Model 14) with the highest average R^2 value for each month all include TRMM3B43 anomaly

434

(Table S17). However, for temperature anomaly during 2000-2019 (Table S17), those models

435

(Model4, Model5 and Model7) that did not consider LST anomaly also exhibited excellent

436

performance.

437

Our results demonstrated that ChinaClim_timeseries showed excellent performance during 1952-

438

2019 (Table 4). Precipitation had an average R^2 of 0.699-0.923, an average $RMSE$ between 7.449



439 mm and 56.756 mm, and an average of *MAE* of 4.263–40.271 mm for all months. Similarly, in terms
 440 of seasonal changes, compared with other months, the accuracy of precipitation was slightly worse
 441 from Jun to Sep. Average temperature had an average R^2 of 0.966–0.985, an average *RMSE* between
 442 0.807 °C and 1.394 °C, and an average *MAE* of 0.548–0.930 °C for all months. Maximum
 443 temperature had an average R^2 of 0.939–0.981, an average *RMSE* between 0.935 °C and 1.391 °C,
 444 and an average *MAE* of 0.608°C ~0.877 °C for all months. Minimum temperature had an average
 445 R^2 of 0.968–0.977, an average *RMSE* between 0.924 °C and 1.766 °C, and an average *MAE* of
 446 0.641~1.236 °C for all months. The performance of the average temperature was the best, followed
 447 by the maximum temperature and the minimum temperature.

448 Table 4. Tenfold cross-validation statistics for ChinaClim_timeseries during 1952-2019.

		Jan	Feb	Mar	Apr	May	Jun	Jul	Aug	Sep	Oct	Nov	Dec
Precipitation	R^2	0.898	0.917	0.921	0.887	0.855	0.799	0.710	0.699	0.746	0.809	0.838	0.845
	<i>RMSE</i>	7.512	9.714	15.326	24.374	36.983	49.620	56.806	54.126	37.955	22.966	13.751	7.592
	<i>MAE</i>	4.370	5.643	9.134	15.111	23.608	33.319	40.403	37.727	24.938	13.857	7.955	4.320
Average temperature	R^2	0.981	0.980	0.978	0.974	0.967	0.966	0.972	0.974	0.976	0.980	0.985	0.983
	<i>RMSE</i>	1.394	1.286	1.091	0.953	0.933	0.888	0.820	0.807	0.846	0.909	1.027	1.268
	<i>MAE</i>	0.930	0.859	0.736	0.653	0.627	0.584	0.554	0.548	0.589	0.636	0.722	0.866
Maximum temperature	R^2	0.977	0.973	0.966	0.953	0.939	0.941	0.951	0.958	0.961	0.967	0.980	0.981
	<i>RMSE</i>	1.391	1.350	1.242	1.144	1.116	1.065	0.987	0.940	0.935	1.010	1.075	1.249
	<i>MAE</i>	0.877	0.870	0.825	0.769	0.743	0.704	0.685	0.647	0.608	0.647	0.697	0.801
Minimum temperature	R^2	0.975	0.977	0.976	0.975	0.971	0.968	0.972	0.973	0.973	0.976	0.979	0.976
	<i>RMSE</i>	1.766	1.600	1.332	1.110	1.067	1.008	0.924	0.949	1.045	1.167	1.357	1.637
	<i>MAE</i>	1.236	1.125	0.902	0.803	0.770	0.703	0.641	0.666	0.753	0.852	0.979	1.160

449 4.2.2 Comparison of ChinaClim_timeseries to other datasets

450 Here, we compared the accuracy of ChinaClim_timeseries with Peng’s climate surface (Peng et al.,
 451 2019) and CHELSAcruts (Karger et al., 2017) by R^2 , *RMSE* and *MAE* in China and four climate
 452 zones (temperate continental, high cold Tibetan Plateau, temperate monsoonal and subtropical-
 453 tropical monsoonal climate zones). The independent weather stations extracted from a tenfold cross-



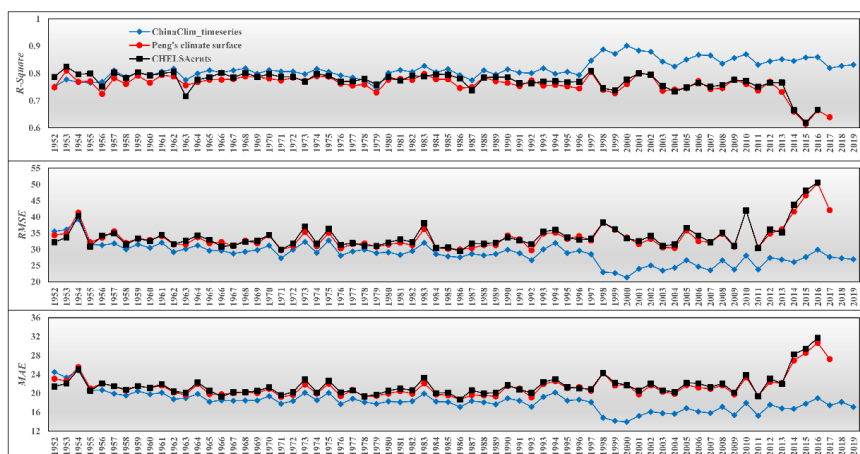
454 validation approach were used to diagnose the performance of ChinaClim_timeseries, while only
 455 these independent weather stations from CMD with small deviations (< 200 m) between the
 456 recorded and actual elevation (1 km DEM) were used to assess the accuracy of CHELSAcruts and
 457 Peng's climate surface.

458 The accuracy of ChinaClim_timeseries for precipitation estimation showed better performance than
 459 Peng's climate surface and CHELSAcruts in China with R^2 increased by 6.15 % and 5.68 %, $RMSE$
 460 decreased by 14.71 % and 15.36 % and MAE decreased by 15.15 % and 16.22 %, respectively (Table
 461 5). Specifically, ChinaClim_timeseries and CHELSAcruts showed similar accuracy in Temperate
 462 continental; although ChinaClim_timeseries had a slightly lower R^2 than CHELSAcruts,
 463 CHELSAcruts had higher $RMSE$ and MAE . Moreover, ChinaClim_timeseries in high cold Tibetan
 464 Plateau, R^2 increased by 13.08 % and 15.87 %, $RMSE$ decreased by 27.46 % and 32.97 % and MAE
 465 decreased by 23.13 % and 30.81 %, respectively. Compared with CHELSA_cruts, except the R^2 of
 466 our product was slightly lower in the temperate continental, all indicators were obviously better in
 467 different zones, especially in high cold Tibetan Plateau and subtropical-tropical monsoonal.
 468 Remarkably, in terms of interannual variations (Fig.12), ChinaClim_timeseries performed slightly
 469 better than other datasets before 1998, while its accuracy was greatly improved during 1998-2019.

470 Table 5. The overall accuracy of precipitation for ChinaClim_timeseries, Peng's climate surface and CHELSAcruts in China and four
 471 climate zones

	Precipitation	R^2	$RMSE$	MAE
China	ChinaClim_timeseries	0.855	33.868	18.063
	Peng's climate surface	0.805	39.707	21.290
	CHELSAcruts	0.809	40.015	21.560
temperate continental climate	ChinaClim_timeseries	0.822	14.805	7.729
	Peng's climate surface	0.791	16.575	8.881
	CHELSAcruts	0.832	15.043	7.892
high cold Tibetan Plateau	ChinaClim_timeseries	0.807	22.942	12.454
	Peng's climate surface	0.714	31.625	16.201
	CHELSAcruts	0.696	34.228	18.000
temperate monsoonal	ChinaClim_timeseries	0.851	26.222	13.588
	Peng's climate surface	0.817	29.151	15.496
	CHELSAcruts	0.831	28.819	15.375
subtropical-tropical monsoonal	ChinaClim_timeseries	0.820	45.501	27.502
	Peng's climate surface	0.758	52.426	31.612
	CHELSAcruts	0.760	52.950	32.364

472



473
474 Figure 12. The accuracy of interannual variations in ChinaClim_timeseries, Peng's climate surface and
475 CHERSAcruTs for precipitation. The accuracy of ChinaClim_timeseries for temperatures estimation also showed better performance
476 than Peng's climate surface and CHERSAcruTs in China and different climate zones (Tables 6-7).
477 In China, the R^2 , $RMSE$ and MAE of maximum temperature were 0.989, 1.167 °C and 0.724 °C,
478 respectively, and those of minimum temperature were 0.989, 1.303 °C and 0.892°C, respectively.
479 Our results showed that all R^2 were very high among three datasets, but compared to Peng's and
480 CHERSAcruTs, our $RMSE$ decreased by 10.17 % and 19.14 % for maximum temperature, and by
481 8.37 % and 14.42 % for minimum temperature; MAE decreased by 25.73 % and 34.02 % for
482 maximum temperature and by 16.92 % and 20.74 % for minimum temperature. In different climate
483 zones, the accuracy of ChinaClim_timeseries was much better than Peng's climate surface and
484 CHERSAcruTs. Especially in the High cold Tibetan Plateau, our $RMSE$ decreased by 23.31 % and
485 36.52 % for maximum temperature and by 21.61 % and 9.65 % for minimum temperature,
486 respectively; our MAE decreased by 39.61 % and 50.00 % for maximum temperature and by 29.35 %
487 and 16.81 % for minimum temperature, respectively. Moreover, in terms of interannual variation
488 (Figs 13-14), our results demonstrated that despite the accuracy of Peng's climate surface and
489 CHERSAcruTs also very well with high R^2 , ChinaClim_timeseries undoubtedly showed more
490 powerful performance in almost all years with lower $RMSE$ and MAE .

491
492
493



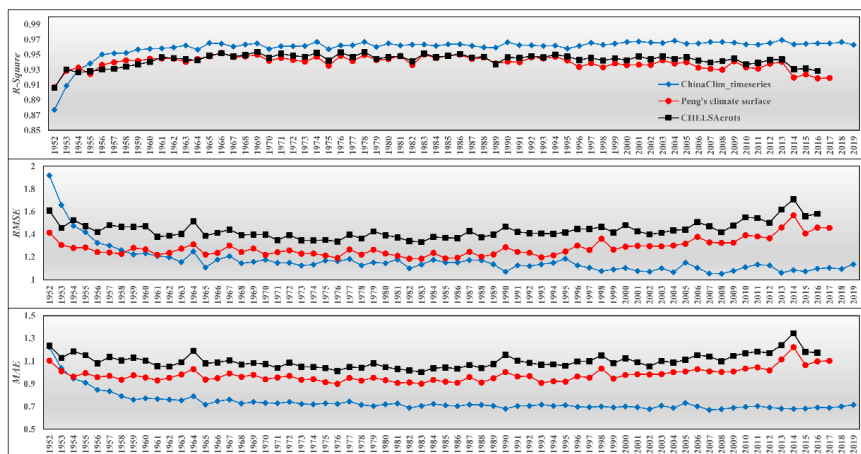
494 Table 6. The overall accuracy of maximum temperature for ChinaClim_timeseries, Peng's climate surface and CHELSAcruts in China
 495 and four climate zones.

	Maximum temperature	<i>R2</i>	<i>RMSE</i>	<i>MAE</i>
China	ChinaClim_timeseries	0.989	1.167	0.724
	Peng's climate surface	0.988	1.299	0.974
	CHELSAcruts	0.987	1.443	1.097
temperate continental	ChinaClim_timeseries	0.989	1.346	0.799
	Peng's climate surface	0.985	1.591	1.202
	CHELSAcruts	0.981	1.835	1.358
high cold Tibetan Plateau	ChinaClim_timeseries	0.958	1.705	1.115
	Peng's climate surface	0.951	2.224	1.847
	CHELSAcruts	0.947	2.686	2.231
temperate monsoonal	ChinaClim_timeseries	0.996	0.766	0.519
	Peng's climate surface	0.993	1.090	0.847
	CHELSAcruts	0.993	1.225	0.962
subtropical-tropical monsoonal	ChinaClim_timeseries	0.980	1.107	0.712
	Peng's climate surface	0.978	1.252	0.935
	CHELSAcruts	0.980	1.314	1.035

496 Table 7. The overall accuracy of minimum temperature for ChinaClim_timeseries, Peng's climate surface and CHELSAcruts in China and
 497 four climate zones.
 498

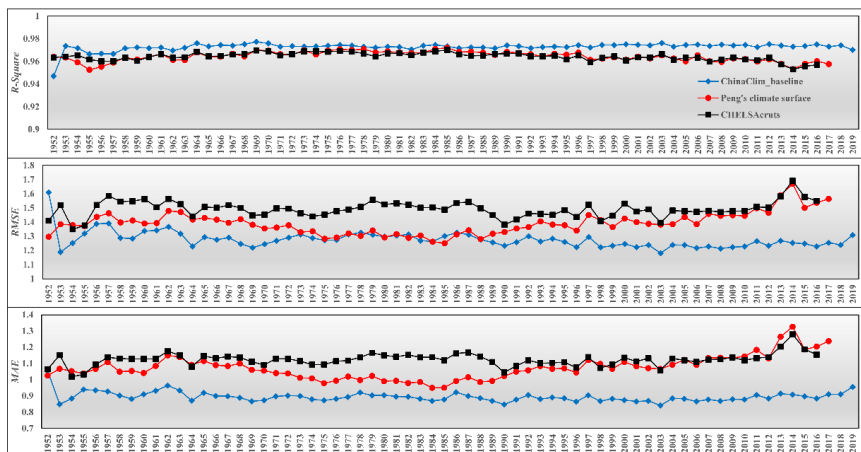
	Minimum temperature	<i>R2</i>	<i>RMSE</i>	<i>MAE</i>
China	ChinaClim_timeseries	0.989	1.303	0.892
	Peng's climate surface	0.988	1.422	1.074
	CHELSAcruts	0.987	1.523	1.125
temperate continental	ChinaClim_timeseries	0.979	1.770	1.270
	Peng's climate surface	0.982	1.765	1.351
	CHELSAcruts	0.976	2.004	1.461
high cold Tibetan Plateau	ChinaClim_timeseries	0.966	1.784	1.271
	Peng's climate surface	0.944	2.276	1.800
	CHELSAcruts	0.958	1.975	1.528
temperate monsoonal	ChinaClim_timeseries	0.992	1.202	0.871
	Peng's climate surface	0.991	1.324	1.032
	CHELSAcruts	0.989	1.585	1.196
subtropical-tropical monsoonal	ChinaClim_timeseries	0.987	0.885	0.621
	Peng's climate surface	0.977	1.254	0.938
	CHELSAcruts	0.984	1.119	0.878

499



500
 501
 502

Figure 13. The accuracy of interannual variations in ChinaClim_timeseries, Peng's climate surfaces and CHELSAcruts for maximum temperature.



503
 504
 505
 506
 507
 508
 509

Figure 14. The accuracy of interannual variations in ChinaClim_timeseries, Peng's climate surface and CHELSAcruts for minimum temperature.



510 **5 Data availability**

511 ChinaClim_baseline is a brand-new and high-quality baseline climatology surface for China at
512 spatial resolution of 1km. The data now is freely available through Zenodo at
513 <https://doi.org/10.5281/zenodo.4287824> (Gong, 2020a), which can be downloaded in TIFF
514 format. The scale factor of the data is 0.01.

515 ChinaClim_timeseries is a monthly temperatures and precipitation dataset in China for the period
516 of 1952-2019 of 1km spatial resolution. The data now are freely available through Zenodo at
517 <https://doi.org/10.5281/zenodo.4288388> (Gong, 2020b) , <https://doi.org/10.5281/zenodo.4288390>
518 (Gong, 2020c) and <https://doi.org/10.5281/zenodo.4288392> (Gong, 2020d), which can be
519 downloaded in TIFF format. The scale factor of the data is 0.1.

520

521

522

523

524

525

526

527

528

529

530

531

532

533

534

535

536

537



538 **6 Discussion**

539 There are a number of baseline climatology surface products for global land surface (Hijmans et al.,
540 2005; Karger et al., 2017; New et al., 1999; New et al., 2002; Fick et al., 2017), while few weather
541 stations are employed to generate these surfaces in China, which might result in insufficient
542 accuracy of these surfaces, and further affect the availability of long-term climate datasets with these
543 surfaces as input. Application TPS algorithm, we considered much more weather stations and
544 satellite-driven variables in climate interpolation to create baseline climatology surface.

545 The precipitation estimation of ChinaClim_baseline performed well in all months with R^2 greater
546 than 0.86. The *RMSEs* and *MAEs* in summer (Jun-Aug) were much higher than other months, which
547 is also reported by the previous studies that the estimation of summer precipitation is pretty difficult
548 than that of winter precipitation, especially in the monsoon zones (Chen et al., 2018; Fick et al.,
549 2017). It is because summer precipitation is deeply affected by summer monsoon. However,
550 compared to WorldClim2 and CHELSA, ChinaClim_baseline deeply improved the accuracy of
551 precipitation with higher R^2 , lower *RMSE*, and *MAE*, especially in temperate continental and high
552 cold Tibetan Plateau zones and summer months. Because ChinaClim_baseline used much more
553 weather stations, and the spatially continuous satellite-driven TRMM3B43 which can distinguish
554 the rain shadow effect of mountains and provide enough information in sparse areas of weather
555 station, while WorldClim2 and CHELSA cannot (Deblauwe et al., 2016). Moreover, our models
556 constructed by each month could well reveal the seasonal variation of precipitation. So, our work
557 could provide a good reference for accurately estimating precipitation (especially for precipitation
558 in rainy season), which allows us to better understand the hydrological processes and execute more
559 meaningful ecological modeling based on ChinaClim_baseline.

560 The accuracy of the average temperature was the best, followed by the maximum temperature, and
561 the minimum temperature. In the meantime, the accuracy of summer temperatures was better than
562 winter temperatures. It is not difficult to understand that summer temperature and maximum
563 temperature often simply changes with elevation, while winter temperature, and minimum
564 temperature, have a more complex relationship with elevation (Daly et al., 2008; Gustavsson et al.,
565 1998). CHELSA simply used temperature lapse rates to estimate temperatures, which might make



566 mistakes in temperature estimations without sufficient weather stations for corrections in high-
567 altitude regions. Although WorldClim2 considered LST, it did not consider the effects of LST on
568 the model accuracy for each month (Hijmans et al., 2005; Fick et al., 2017), which ignored the
569 improvements helped by LST during key months such as vegetation growth season; In comparison
570 with WorldClim2 and CHELSA, our model deeply improved the accuracy of temperature element
571 during growing season facilitated by select optimal multiple model formulations for each month,
572 which is very important for revealing the vegetation-climate relationship. Previous findings claimed
573 that models only using latitude, longitude, elevation can be consistently superior for temperatures
574 estimation (Parmentier et al., 2014), while our results showed that LST can greatly improve the
575 accuracy of temperatures estimation, especially in summer months. Some studies showed that LST
576 just improved the estimates for maximum temperature (Kilibarda et al., 2014), while our results
577 found that LST improved not only the estimate of maximum temperature, but also the estimates of
578 average and minimum temperature was greatly improved.

579 There was a large amount of evidence to suggested that the CAI method can better generate long-
580 term monthly climate surface (Abatzoglou et al., 2018; Becker et al., 2013; C. Vega et al., 2017;
581 Karger et al., 2017; Mosier et al., 2014; Peng et al., 2019; Willmott and Robeson, 2010). Our results
582 proved Peng's climate surface and CHELSAcruts datasets, relying on coarse CRU anomaly and
583 high-quality baseline climatology surfaces with CAI method, had relatively high accuracy (high R^2)
584 with a few weather stations in China at 1km spatial resolution. (Karger et al., 2017; Peng et al.,
585 2019). However, those studies rarely incorporated satellites-driven products into climate
586 interpolation, and the performance of baseline climatology surface covering China (WorldClim2
587 and CHELSA) using the CAI method was also troubling, especially in high cold Tibetan Plateau.
588 ChinaClim_timeseries used a higher precision baseline climatology surface (ChinaClim_baseline)
589 as input in CAI method. We also implemented TPS interpolation by selecting optimal multiple
590 model formulations for each month. Not only can we make full use of the time-series weather
591 stations, but also consider the satellites-driven anomaly as either independent spline variables or
592 linear covariates to further improve the accuracy of the final monthly climate surface. Our results
593 showed that ChinaClim_timeseries was indeed a better climate dataset than Peng's climate surface
594 and CHELSAcruts in China with higher R^2 , and lower $RMSE$ and MAE , especially in high cold



595 Tibetan Plateau for precipitation estimation, R^2 increased by 13.08 % and 15.87 %, $RMSE$ decreased
596 by 27.46 % and 32.97 % and MAE decreased by 23.13 % and 30.81 %, respectively.

597 Previous studies indicated that baseline climatology surface, considering detailed topographic
598 information, the effects of distance to the nearest coast and satellite-driven variables, is physically
599 representative and has a fine-scale distribution of meteorological variables (Marchi et al., 2019;
600 Mosier et al., 2014; Peng et al., 2017; Platts et al., 2015). Thus, a superior baseline climatology
601 surface is helpful to improve the accuracy of the long-term monthly climate surface. In this study,
602 the baseline climatology surface was not only used as one of the inputs of CAI method, but also as
603 one of the variables of TPS models to calculate the monthly anomaly surface. Our results showed
604 that TPS models considering baseline climatology surface, showed better performance for
605 precipitation and temperatures anomaly in all months during 1952-2019 (Table S12 and S17), which
606 was helpful to improve the estimates of ChinaClim_timeseries. However, in terms of interannual
607 variation, compared with other datasets, the estimates of ChinaClim_timeseries for precipitation
608 performed slightly better during 1952-1997, while the performance was much better during 1998-
609 2019 (Fig.12). Owing to the utilization of satellite-driven TRMM3B43 anomaly in climate
610 interpolation after 1997, we believed that satellite-driven anomaly can greatly improve the estimates
611 of precipitation and baseline climatology surface only slightly improve the estimates of precipitation.
612 Remarkably, we only considered satellites-driven TRMM3B43 anomaly as either independent
613 spline variables or linear covariates to generate the final monthly precipitation surface and this
614 process was not implemented in the temperature estimation because the optimal TPS model did not
615 reveal that LST anomaly can effectively improve the temperature estimation (Table S17). The
616 temperatures estimation of ChinaClim_timeseries still performed well during 1952-2019 (Figs 13-
617 14), which might be attributed to a better baseline climatology surface as input in CAI method.
618 Although previous studies illustrated that satellites-driven products can greatly improve the
619 accuracy of climate elements estimation (Kilibarda et al., 2014; Kolios and Kalimeris, 2020; Yao et
620 al., 2020), our results showed that satellite-driven anomaly cannot substantially improve the
621 estimates of temperatures and baseline climatology surface can play a key role in long-term
622 temperature estimation.

623 As shown above, ChinaClim_baseline is a brand-new and high-quality baseline climatology surface



624 in China currently released. Baseline climatology surface, not only could be applied in history and
625 paleo climate models, but also can be combined with GCM products to generate future climate
626 change scenarios with high resolution (Peng et al., 2019; Platts et al., 2015). Besides, the quality of
627 baseline climatology surface has a fundamental role in predictions of the potential impact of climate
628 change on organisms and natural ecosystems (Marchi et al., 2019, Vega et al 2017).
629 ChinaClim_timeseries is a very high-quality monthly climate surface and can successfully reveal
630 the spatial-temporal change patterns of precipitation and temperatures for China. At the same time,
631 it can be used as a good data source for long-term modeling of hydrology, ecology, and other related
632 fields. In particular, ChinaClim_timeseries also could help to reduce the uncertainty of the input of
633 climate parameters in high cold Tibetan Plateau zones, and better quantify the region's ecosystem
634 variation in the context of global changes.

635 The TRMM3B43 improves the estimate of precipitation, while the 0.25 degree resolution of TRMM
636 might be fail to represent many important finer-scale climatic features due to the uncertainties
637 caused by the simply resampling process from 0.25 degree to 1km (Deblauwe et al., 2016). In the
638 meantime, MODIS-LST was effective to improve the algorithms for estimating air temperatures
639 (Jin and Dickinson, 2010; Mildrexler et al., 2011; Parmentier et al., 2014; Yao et al., 2020). However,
640 land surface temperature is tightly related to land cover, which is itself highly affected by human
641 activities. Therefore, incorporating TRMM3B43 and LST into the generation of
642 ChinaClim_baseline and ChinaClim_timeseries maybe present challenges (Deblauwe et al., 2016).
643 Besides, it should also be noted that there is a temporal mismatch between the datasets from weather
644 stations (1980–2010) and from average TRMM3B43 (1998-2019) and LST (2001–2019) in
645 estimating ChinaClim_baseline. With the emergence of high-resolution and long-term climate
646 remote sensing products in the future, and the improvement of multiple remote sensing data fusion
647 technology, we could greatly reduce the uncertainty of climate interpolation and improve the
648 accuracy of product estimation, particularly in places with very few weather stations or strong
649 gradients change or complex terrain (Immerzeel et al., 2009; Li and Shao, 2010; Fick et al., 2017;
650 Vega et al 2017). Although our research showed that TPS method could be used well in climate
651 interpolation, many studies have pointed out that this method accounted for direct elevation effects
652 only, and had difficulty in considering the sharp changes in the relationship between climate and



653 elevation (Daly et al., 2008; Daly et al., 2007; Marchi et al., 2019). Therefore, it is essential to
654 comprehensively quantify the non-linear relationship between environmental variables and climate
655 elements. Thus, future work ought to couple these nonlinear relationships with TPS or new
656 algorithm for the better estimates of climate elements.

657

658

659

660

661

662

663

664

665

666

667

668 **Author Contributions.** Haibo Gong formed the original idea and wrote the original manuscript;
669 Huiyu Liu offered valuable comments and was responsible for the manuscript revisions; Xueqiao
670 Xiang and Xiaojuan Xu participated in the data collection and analysis; FuSheng Jiao and Zhenshan
671 Lin created figures and tables.

672

673 **Competing interests.** The author declare that they have no conflict of interest

674

675 **Acknowledgements.** We thank the all people and institutions who contributed to the establishment
676 of this dataset

677

678 **Financial support.** This research had been funded by the National Natural Science Foundation of
679 China (No. [41971382](#), [31870454](#)) and the Priority Academic Program Development of Jiangsu
680 Higher Education Institutions ([164320H116](#)).



681 **References**

- 682 Abatzoglou, J.T., Dobrowski, S.Z., Parks, S.A., and Hegewisch, K.C.: TerraClimate, a high-resolution global dataset of monthly
683 climate and climatic water balance from 1958–2015, *Scientific Data.*, 5,170191, 2018.
- 684 Becker, A., et al.: A description of the global land-surface precipitation data products of the Global Precipitation Climatology
685 Centre with sample applications including centennial (trend) analysis from 1901–present, *Earth System Science Data.*,
686 5,1(2013-02-21), 5(1), 921-998, 2013.
- 687 Belda, M., Holtanova, E., Kalvova, J., and Halenka, T.: Global warming-induced changes in climate zones based on CMIP5
688 projections, *Climate Research.*, 71(1), 17-31, 2017.
- 689 Biasutti, M., Yuter, S.E., Burleyson, C.D., and Sobel, A.H.: Very high resolution rainfall patterns measured by TRMM precipitation
690 radar: seasonal and diurnal cycles, *Climate Dynamics.*, 39(1), 239-258, 2012.
- 691 Boer, E.P.J., Beurs, K.M.de., and Hartkamp, A.D.: Kriging and thin plate splines for mapping climate variables, *International
692 Journal of Applied Earth Observation and Geoinformation.*, 3(2), 146-154, 2001.
- 693 Vega, G.C., Pertierra, L.R., and Olalla-Tárraga, M.Á.: MERRAclim, a high-resolution global dataset of remotely sensed bioclimatic
694 variables for ecological modelling, *Scientific Data.*, 4(1), 170078, 2017.
- 695 Chaney, N.W., Sheffield, J., Villarini, G., and Wood, E.F.: Development of a High-Resolution Gridded Daily Meteorological
696 Dataset over Sub-Saharan Africa: Spatial Analysis of Trends in Climate Extremes, *Journal of Climate.*, 27(15), 5815-
697 5835, 2014.
- 698 Chen, Y., et al.: A new downscaling-integration framework for high-resolution monthly precipitation estimates: Combining rain
699 gauge observations, satellite-derived precipitation data and geographical ancillary data, *Remote Sensing of
700 Environment.*, 214, 154-172, 2018.
- 701 Daly, C., Gibson, W.P., Taylor, G.H., Johnson, G.L., and Pasteris, P.: A knowledge-based approach to the statistical mapping of
702 climate, *Climate Research.*, 22(2), 99-113, 2002.
- 703 Daly, C., et al.: Physiographically sensitive mapping of climatological temperature and precipitation across the conterminous
704 United States, *International Journal of Climatology.*, 28(15), 2008.
- 705 Daly, C., Smith, J.W., Smith, J.I., and Mckane, R.B.: High-Resolution Spatial Modeling of Daily Weather Elements for a Catchment
706 in the Oregon Cascade Mountains, United States, *Journal of Applied Meteorology & Climatology.*, 46(10): 1565-1586,
707 2007.
- 708 Deblauwe, V., et al.: Remotely sensed temperature and precipitation data improve species distribution modelling in the tropics,
709 *Global Ecology & Biogeography*; 25(4): 443-454, 2016.
- 710 Gao, L., et al.: A high-resolution air temperature data set for the Chinese Tian Shan in 1979–2016, *Earth Syst. Sci. Data.*, 10(4):
711 2097-2114, 2018.
- 712 Gong, H.: A Brand-New and High-Quality Baseline Climatology Surface for China (ChinaClim_baseline), Zenodo,
713 <https://doi.org/10.5281/zenodo.4287824>, 2020a
- 714 Gong, H.: 1 km Monthly Precipitation Dataset for China from 1952 to 2019 (ChinaClim_timeseries), Zenodo,
715 <https://doi.org/10.5281/zenodo.4288388>, 2020b
- 716 Gong, H.: 1 km Monthly Maximum Temperature Dataset for China from 1952 to 2019 (ChinaClim_timeseries), Zenodo,
717 <https://doi.org/10.5281/zenodo.4288390>, 2020c
- 718 Gong, H.: 1 km Monthly Minimum Temperature Dataset for China from 1952 to 2019 (ChinaClim_timeseries), Zenodo,
719 <https://doi.org/10.5281/zenodo.4288392>, 2020d
- 720 Gustavsson, T.R., Karlsson, M., Bogren, J.R., and Lindqvist, S.: Development of Temperature Patterns during Clear Nights, *J. Appl.
721 Meteorol.*, 37(6): 559-571, 1998.
- 722 Hamann, A., Roberts, D.R., Barber, Q.E., Carroll, C., and Nielsen, S.E.: Velocity of climate change algorithms for guiding



- 723 conservation and management, *Glob. Change Biol.*, 21(2): 997-1004, 2015.
- 724 Harris, I., Jones, P.D., Osborn, T.J., and Lister, D.H.: Updated high-resolution grids of monthly climatic observations - the CRU
725 TS3.10 Dataset, *International Journal of Climatology.*, 34(3): 623-642, 2014.
- 726 Hartkamp, A.D., De Beurs, K., Stein, A., and White, J.W.: *Interpolation Techniques for Climate Variables Interpolation.*, 1999.
- 727 Hijmans, R.J., Cameron, S.E., Parra, J.L., Jones, P.G., and Jarvis, A.: Very high resolution interpolated climate surfaces for global
728 land areas, *International Journal of Climatology.*, 25(15): 1965-1978, 2005.
- 729 Huffman, G.J., Adler, R.F., Bolvin, D.T., and Nelkin, E.J.: The TRMM Multisatellite Precipitation Analysis (TMPA): Quasi-Global,
730 Multiyear, Combined-Sensor Precipitation Estimates at Fine Scales. *J. hydrometeor.*, 2010.
- 731 Hutchinson, M.F.: Interpolating mean rainfall using thin plate smoothing splines. *International Journal of Geographical Information
732 Systems*, 9(4): 385-403, 1995.
- 733 Hutchinson, M.F., Xu T.: *ANUSPLIN Version 4.4 User Guide*. Australian National University: Canberra., 2013.
- 734 Immerzeel, W.W., Rutten, M.M., and Droogers, P.: Spatial downscaling of TRMM precipitation using vegetative response on the
735 Iberian Peninsula, *Remote Sensing of Environment.*, 113(2): 362-370, 2009.
- 736 Jin, M., and Dickinson, R.E.: Land surface skin temperature climatology: benefitting from the strengths of satellite observations,
737 *Environmental Research Letters.*, 5(4): 44004, 2010.
- 738 Karger, D.N., et al.: Climatologies at high resolution for the earth's land surface areas, *Scientific Data.*, 4(1),170122, 2017.
- 739 Kilbarda, M., et al.: Spatio-temporal interpolation of daily temperatures for global land areas at 1 km resolution, *Journal of
740 Geophysical Research: Atmospheres.*, 119(5), 2294-2313, 2014.
- 741 Kolios, S., and Kalimeris, A.: Evaluation of the TRMM rainfall product accuracy over the central Mediterranean during a 20-year
742 period (1998–2017), *Theoretical and Applied Climatology.*, 139(1): 785-799, 2020.
- 743 Lawrimore, J.H., et al.: An overview of the Global Historical Climatology Network monthly mean temperature data set, version 3,
744 *Journal of Geophysical Research Atmospheres.*, 116(D19), 2011.
- 745 Li, M., and Shao, Q.: An improved statistical approach to merge satellite rainfall estimates and raingauge data, *Journal of
746 Hydrology.*, 385(1-4): 51-64, 2010.
- 747 Liu, Q., et al.: The hydrological effects of varying vegetation characteristics in a temperate water-limited basin: Development of
748 the dynamic Budyko-Choudhury-Porporato (dBCP) model, *Journal of Hydrology.*, 595-611, 2016.
- 749 Marchi, M., Sinjur, I., Bozzano, M., and Westergren, M.: Evaluating WorldClim Version 1 (1961-1990) as the Baseline for
750 Sustainable Use of Forest and Environmental Resources in a Changing Climate, *Sustainability.*, 11(11): 14, 2019.
- 751 Michaelides, S., et al.: Precipitation: Measurement, remote sensing, climatology and modeling, *Atmospheric Research.*, 94(4): 512-
752 533, 2009.
- 753 Mildrexler, D.J., Zhao, M., and Running, S.W.: A global comparison between station air temperatures and MODIS land surface
754 temperatures reveals the cooling role of forests. *116(G3)* , 2011.
- 755 Mosier, T.M., Hill, D.F., and Sharp, K.V.: 30-Arcsecond monthly climate surfaces with global land coverage, *International Journal
756 of Climatology.*, 34(7) , 2014.
- 757 Muller, R.A., Rohde, R., Jacobsen, R., Muller, E., and Wickham, C.: A New Estimate of the Average Earth Surface Land
758 Temperature Spanning 1753 to 2011, 2013.
- 759 New, M., Hulme, M., and Jones, P.: Representing Twentieth-Century Space–Time Climate Variability. Part I: Development of a
760 1961–90 Mean Monthly Terrestrial Climatology, *Journal of Climate.*, 12(3): 829-856, 1999.
- 761 New, M., Lister, D., Hulme, M., and Makin, I.: A high-resolution data set of surface climate over global land areas, *Climate
762 Research.*, 21(1): 1-25, 2002.
- 763 Parmentier, B., et al.: An Assessment of Methods and Remote-Sensing Derived Covariates for Regional Predictions of 1 km Daily
764 Maximum Air Temperature, *Remote Sensing.*, 6(9): 8639-8670, 2014.
- 765 Peng, S., Ding, Y., Liu, W., and Li, Z.: 1 km monthly temperature and precipitation dataset for China from 1901 to 2017, *Earth
766 Syst. Sci. Data.*, 11(4): 1931-1946, 2019.



- 767 Peng, S., et al.: Spatiotemporal change and trend analysis of potential evapotranspiration over the Loess Plateau of China during
768 2011–2100, *Agricultural and Forest Meteorology*, 233: 183-194, 2017.
- 769 Pfister, L., et al.: Statistical reconstruction of daily precipitation and temperature fields in Switzerland back to 1864, *Clim. Past*,
770 16(2): 663-678, 2020.
- 771 Platts, P.J., Omeny, P.A., and Marchant, R.: AFRICLIM: high - resolution climate projections for ecological applications in Africa,
772 *African Journal of Ecology*, 53(1), 103-108, 2015.
- 773 Ray, D., et al.: Comparing the provision of ecosystem services in plantation forests under alternative climate change adaptation
774 management options in Wales, *Reg. Envir. Chang.*, 15(8): 1501-1513, 2015.
- 775 Simpson, J., Kummerow, C., Tao, W.K., and Adler, R.F.: The Tropical Rainfall Measuring Mission (TRMM) Sensor Package,
776 *Meteorology & Atmospheric Physics*, 60(1-3): 19-36, 1996.
- 777 Siuki, S.K., Saghafian, B., and Moazami, S.: Comprehensive evaluation of 3-hourly TRMM and half-hourly GPM-IMERG satellite
778 precipitation products, *International Journal of Remote Sensing*, 38(1-2): 558-571, 2017.
- 779 Fick, S.E., and Hijmans, R.J.: WorldClim 2: new 1-km spatial resolution climate surfaces for global land areas, *International Journal*
780 *of Climatology*, 37(12), 4302-15, 2017.
- 781 Sterl, A., Komen, G.J., and Cotton, P.D.: Fifteen years of global wave hindcasts using winds from the European Centre for Medium-
782 Range Weather Forecasts reanalysis: Validating the reanalyzed winds and assessing the wave climate, *Journal of*
783 *Geophysical Research Oceans*, 103, 5477-5492, 1998.
- 784 Thornton, P.E., Running, S.W., and White, M.A.: Generating surfaces of daily meteorological variables over large regions of
785 complex terrain, *Journal of Hydrology*, 190(3-4): 214-251, 1997.
- 786 Willmott, C.J., and Robeson, S.M.: Climatologically aided interpolation (CAI) of terrestrial air temperature, *International Journal*
787 *of Climatology*, 15(2), 2010.
- 788 Wu, T., and Li, Y.: Spatial interpolation of temperature in the United States using residual kriging, *Applied Geography*, 44: 112-
789 120, 2013.
- 790 Yao, R., Wang, L., Huang, X., Li, L., and Jiang, W.: Developing a temporally accurate air temperature dataset for Mainland China,
791 *Science of The Total Environment*, 706, 136037, 2020.
- 792